# Measurements of Non-Maxwellian Electron Distribution Functions and Their Effect on Laser Heating

A. L. Milder, J. Katz, R. Boni, J. P. Palastro, M. Sherlock, W. Rozmus, and D. H. Froula

# Measurements of non-Maxwellian electron distribution functions and their effect on laser heating

A. L. Milder,[1,2,*] J. Katz,[1] R. Boni,[1] J. P. Palastro,[1]

M. Sherlock,[3] W. Rozmus,[4] and D. H. Froula[1,2]

[1]*Laboratory for Laser Energetics, 250 E. River Rd, Rochester, NY 14623, USA*

[2]*Department of Physics and Astronomy,*

*University of Rochester, Rochester, NY 14623, USA*

[3]*Lawrence Livermore National Laboratory,*

*7000 East Avenue, Livermore, CA 94550, USA*

[4]*Department of Physics, University of Alberta,*

*Edmonton, Alberta T6G 2E1, Canada*

## Abstract

Electron velocity distribution functions driven by inverse bremsstrahlung heating were measured to be non-Maxwellian using a novel angularly resolved Thomson-scattering instrument and the corresponding reduction of electrons at slow velocities resulted in a $\sim 40\%$ measured reduction in inverse bremsstrahlung absorption. The distribution functions were measured to be super-Gaussian in the bulk ($v/v_{th} < 3$) and Maxwellian in the tail ($v/v_{th} > 3$) when the laser heating rate dominated over the electron-electron thermalization rate. Simulations with the particle code *Quartz* showed the shape of the tail was dictated by the uniformity of the laser heating.

Statistical mechanics governs the fundamental properties of many body systems and the corresponding velocity distributions dictates most material properties. In plasmas, a description through statistical mechanics is challenged by the fact that the movement of one electron effects many others through their Coulomb interactions, leading to collective motion. Although most of the research in plasma physics assumes equilibrium electron distribution functions, or small departures from a Maxwell–Boltzmann (Maxwellian) distribution, this is not a valid assumption in many situations. Deviations from a Maxwellian can have significant ramifications on the interpretation of diagnostic signatures, and more importantly in our ability to understand the basic nature of plasmas. Uncertainties in the distribution function have implications across many areas of plasma physics including magnetic and inertial confinement fusion, astrophysics, and space sciences. The uncertainty in modeling of high-velocity electrons, including their nonlocal behavior, combined with the lack of experimental constraints has led to fundamental questions about the shape of electron velocity distributions.

In 1980, it was predicted that laser heating preferentially transfers energy to the slower electrons driving their velocity distribution to have a flat-top, or super-Gaussian shape[1]. It was shown that this reduction in slow electrons reduces the inverse bremsstrahlung heating rate and in subsequent years nearly all hydrodynamic models that include laser propagation have introduced a factor to adjust the laser absorption due to this effect[2, 3]. Challenges in measuring absorption and the electron distribution function[4–6] have made it difficult to verify these theories, although extensive computational work has been done over the last forty years[7–12].

Several theoretical and computational studies have explored the evolution of the distribu-

tion function resulting from inverse bremsstrahlung heating, including the consideration of the relatively small electron-ion collision rate of the fast electrons [13], thermal transport[8], and electron-electron collisions[9], which all tend to produce high-velocity electrons (tails) and a non-Maxwellian bulk of electrons.

Historically, measurements of the electron velocity distribution function have been elusive. Typically, Thomson-scattering experiments have assumed Maxwellian distribution functions allowing the plasma conditions[4, 6, 14–19] to be extracted from the spectrum scattered off electrons in the bulk (non-collective) or in the tails (collective) of the electron distribution functions[20]. In the non-collective regime, the power scattered at a particular frequency is proportional to the number of electrons with a velocity that Doppler shifts the frequency of the probe laser to the measured frequency. This provides a direct measurement of the electron distribution function, but in practice, the small scattering cross section of the electron and small number of electrons at high velocities limits this technique to measuring electrons in the bulk of the distribution function[4]. In the collective regime, the power scattered into the collective features is dominated by scattering from electrons propagating at velocities near the phase velocity of the electron plasma waves, which can be significantly faster than the thermal velocity. In theory, a measurement of the complete scattering spectrum in either of these configurations could be used to determine the electron distribution function without an assumption on its shape, but in practice signal-to-noise, instrumental response, and dynamic range of instruments have limited measurements of the distribution function to the bulk [21–27] or a predetermined class of distribution functions[5, 6, 28–34].

In this Letter, we present the first measurements of complete electron distributions without any assumptions on their shape or the underlying physics that produced them. A corresponding reduction in laser absorption, compared to classical absorption, of up to 37% was measured when the electron distributions were determined to be super-Gaussian. At these conditions the inverse bremsstrahlung heating dominated over thermalization by electron-electron collisions, and the measured absorption was in reasonable agreement with analytic predictions[1] that are commonly used in hydrodynamic modeling. To enable single-shot temporally and spatially resolved measurements of the electron distribution function over several orders of magnitude, an optical diagnostic was invented that uses the angular dependence of scattering to simultaneously access the non-collective and collective nature of plasmas. This first-principles measurement showed that during significant heating by the
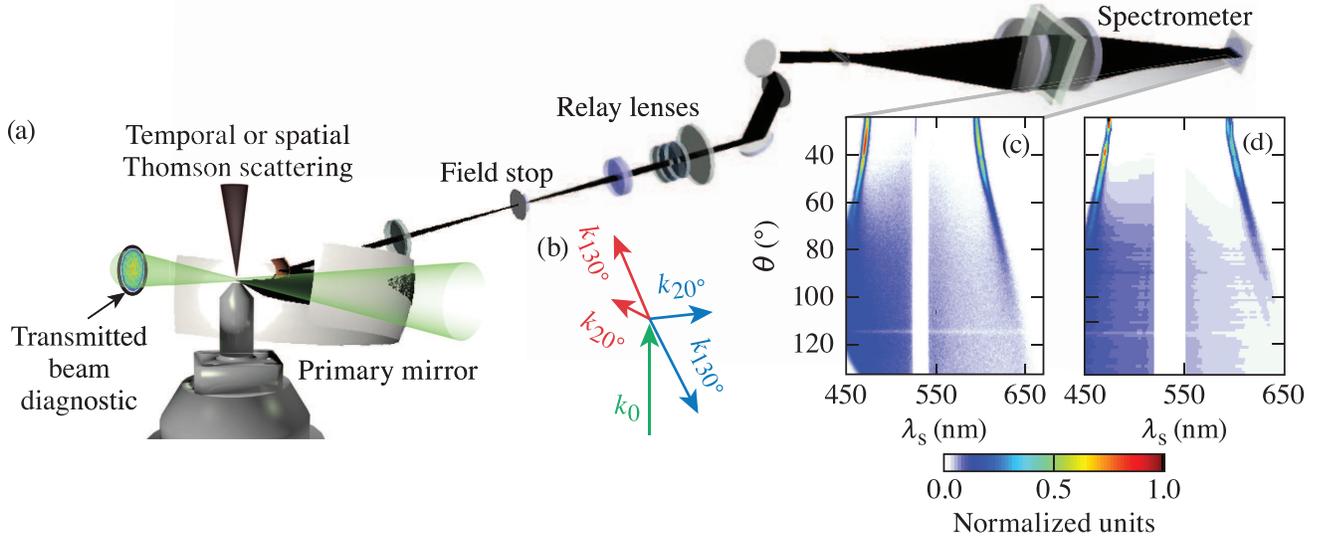
FIG. 1. (a) Experimental setup. The Thomson-scattering probe laser (green) and the view from the temporally or spatially resolved Thomson-scattering instrument (black) are shown. (b) The wave vectors probed by the angularly resolved instrument. (c) Measured and (d) calculated spectra from a krypton plasma.

laser beams, the distributions had a super-Gaussian shape in the bulk ($v < 3v_{th}$) with a Maxwellian tail ($v > 3v_{th}$). The super-Gaussian bulk is associated directly with the inverse bremsstrahlung heating and is well reproduced by the previous computational work[7]. The departure from super-Gaussian at high velocities was predicted by Fourkal *et al.*[9], but these measurements show this deviation at a higher velocity. Particle simulations show improved agreement and demonstrate the importance of isotropic heating in accurately predicting the high-velocity tail.

The Thomson-scattering spectrum, in either the non-collective ($1/k\lambda_D < 1$) or collective ($1/k\lambda_D > 1$) scattering regime, is uniquely dictated by the shape of the electron distribution function ($\lambda_D = v_{th}/\omega_{pe}$, where $v_{th}$ is the electron thermal velocity and $\omega_{pe}$ is the electron plasma frequency). An angularly resolved Thomson-scattering diagnostic was invented [Fig. 1(a)] that allowed the electron distribution function to be determined over nearly five orders of magnitude (Fig. 2). The angular dependence of the Thomson-scattering spectrum was introduced through the wave vector of the fluctuations, $k^2 = k_0^2 + k_s^2 - 2k_0 k_s \cos\theta$, where each angle probed resulted in a spectrum with a different range of frequencies with optimal signal-to-noise. Here, the scattering angle ($\theta$) is the angle between the probe beam ($k_0 = 2\pi/\lambda_0$)

4

and the scattering directions ($k_s = 2\pi/\lambda_s$) [Fig. 1(b)], where $\lambda_0$ and $\lambda_s$ are the probe laser and scattered wavelengths in the plasma, respectively. At each angle, the spectrum is most sensitive to a different part of the distribution function, which allowed the angularly resolved spectrum to define a unique electron distribution function over a large dynamic range.

Experiments were preformed on the OMEGA laser system[35] at the Laboratory for Laser Energetics. A supersonic Mach 3 gas jet [36] with an exit diameter of 2 mm was pressurized with argon, krypton, hydrogen or nitrogen gas to achieve a uniform density neutral gas plume 2 mm above the nozzle. Between five and eleven ultraviolet (UV, 351 nm) laser beams were focused to the center of the gas jet. To generate a uniform plasma, each beam used distributed phase plates, polarization smoothing, and smoothing by spectral dispersion to achieve a uniform overlapped intensity ranging from $I_{UV}^{total} = 0.35 - 2.8 \times 10^{15}$ W/cm$^2$. The energy in the 500-ps full-width at half-maximum (FWHM) flat-top pulse duration of the laser beams was varied from 50 J per beam to 200 J per beam. A green ($\lambda_0 = 526.5$ nm) 200-ps FWHM long probe beam with $\sim$10 J was focused to the center of the plasma. A distributed phase plate was used to produce a flat-top focal spot 100 µm FWHM in diameter ($I_{2\omega} = 6.5 \times 10^{14}$ W/cm$^2$). The rise of the probe beam was delayed either 300 ps or 600 ps from the rise of the heater beams in order to measure the plasma conditions at the end of the heating (300-500 ps) or after the heating beams turned off (600-800 ps). The oscillatory velocity was calculated from the total intensity, $v_{osc}^2$[cm$^2$/s$^2$]$= 739(I_{UV}^{total}$[W/cm$^2$]$/9 + I_{2\omega}$[W/cm$^2$]$/4)$.

To determine the absorption of the probe beam, two high-dynamic range scientific CCD cameras were installed to measure the incident and transmitted energy[37]. The system was capable of measuring 0.1% absorption. On all of the shots reported here, very little beam spray was observed and the transmitted beam was contained well within the measurement region.

Figure 1(c) shows the measured angularly resolved Thomson-scattering spectrum where the ensemble electron motion was encoded on the frequency of the scattered light. To decode the complete electron distribution function (Fig. 2), the light from a 200-ps long, 527-nm laser beam was scattered from and spectrally resolved over a large range of scattering angles (see Supplemental Information A). For the largest scattering angles, the correlation length of the scattering electrons was approximately equal to the electron Debye length of the plasma and the resulting spectrum was strongly influenced by non-collective scattering. By collecting the light at smaller scattering angles, two narrow features at frequencies corresponding
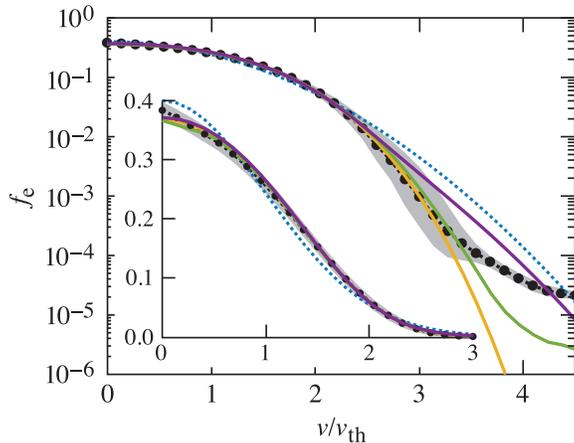
FIG. 2. Electron distributions on linear (inset) and logarithmic scale determined while the laser beams were heating the krypton plasma. The measured distribution (black points) is well reproduced in the bulk by a super-Gaussian function (orange curve) consistent with Matte *et al.* (Eq. 4, m=3.9). A formalism describing the Maxwellian tail from Fourkal *et al.*[9] (purple curve), a Maxwellian distribution (blue curve), and results from particle simulation (green curve) are shown. The 90% confidence interval on the measured distribution function (gray region) is shown.

to the electron-plasma wave resonance become dominant in the spectrum. Measuring the scattering spectrum with continuous angular resolution over 120° has enabled the electron distribution function to be determined out to ~5 times the thermal velocity, which corresponds to a dynamic range of greater than 4 orders of magnitude.

To determine an arbitrary electron distribution function from the angularly resolved Thomson-scattering spectrum, the total power scattered was calculated across the range of scattering angles,

$$P_s(\lambda_s, \theta) = C \left(2\lambda_0/\lambda_s^3 - 1/\lambda_s^2\right) n_e S(x), \tag{1}$$

and compared to the measured spectrum. Here, $n_e$ is the electron density and $C$ is a scale factor. The dynamic form factor in this regime can be approximated by[14],

$$S(x) \simeq \left| \frac{1}{1 + \chi_{Re}[x] + i\chi_{Im}[x]} \right|^2 f_e[x] \tag{2}$$

where $x = \omega/kv_{th}$ is the normalized phase velocity. By assuming the distribution function is isotropic over the range in scattering directions probed, a single projection of the distribution function onto each of the probed vectors was used. To maintain the highest level of generality, the one-dimensional electron distribution function projected along the probed fluctuations

6

was defined as a set of points, $f_e[x]$, where the square brackets are used to denote the discrete domain, which consisted of 64 points. To increase the resolution of the spectral calculation, exponential interpolation of the electron distribution function between the points was used. The real and imaginary parts of the electron susceptibility are given by[38],

$$\chi_{Re} = -\frac{1}{k^2\lambda_D^2}\mathcal{P}\int_{-\infty}^{\infty}\frac{\partial f_e/\partial x'}{x'-x}dx', \; \chi_{Im} = -\frac{\pi}{k^2\lambda_D^2}\frac{\partial f_e}{\partial x'}\Big|_x.$$

The calculated spectrum was convolved with the response functions of the instrument and the measured evolution of the plasma conditions over the 200 ps measurement window (see Supplemental Information A). The resulting synthetic spectrum [e.g., Fig. 1(d)] was compared with the measured spectrum $[P_m(\lambda_s, \theta)]$ by calculating the $\chi^2 = \sum_{\lambda_s}\sum_{\theta}[P_m(\lambda_s, \theta) - P_s(\lambda_s, \theta)]^2/\sigma^2$ over the entire 2-dimensional spectrum, where $\sigma$ is the variation of the data, which was $\sim 5\%$ of the signal for all shots. A gradient descent algorithm[39] was used to find the minimum $\chi^2_{min}$ within the 69 dimensional parameter space, which defined the measured electron distribution function (64 points), plasma conditions ($n_e$ and $T_e$), and scale parameters (3 parameters).

Figure 2 shows the electron distribution function measured while five ultraviolet laser beams, with an overlapped intensity of $I_{UV}^{total} = 2.8\times10^{15}$ W/cm$^2$, uniformly heated a $\sim$1 mm$^3$ volume of gas through inverse bremsstrahlung absorption. As predicted by theory[1], the measurements show that slow electrons are preferentially heated to form a super-Gaussian electron distribution. The measured electron distribution functions are well reproduced in the bulk by the heuristic scaling determined from early Fokker-Plank simulations[7] where the electron distribution functions were parameterized by,

$$f_m(v) = C_m \exp\left[-(v/a_m v_{th})^m\right], \tag{3}$$

with super-Gaussian order

$$m(\alpha) = 2 + \frac{3}{1 + 1.66/\alpha^{0.724}}, \tag{4}$$

$\alpha = Z v_{osc}^2/v_{th}^2$ is the ratio of inverse bremsstrahlung heating rate to electron-electron collision rate and $Z$ the ionization state. Normalization constants ($C_m$, $a_m$) maintain the standard definitions of the first three moments (e.g. $\frac{3}{2}n_e T_e = \int \frac{1}{2}m_e v^2 f_m(v)d^3\mathbf{v}$). For the results shown in Fig. 2, the calculated electron distribution function (Eq. 3) is in excellent agreement with the measurements for velocities less than $\sim 3v_{th}$ when using the overlapped intensity and the measured plasma conditions ($\alpha = 4.3^{+0.7}_{-0.6}$). The plasma conditions ($T_e = 1.16$ keV,
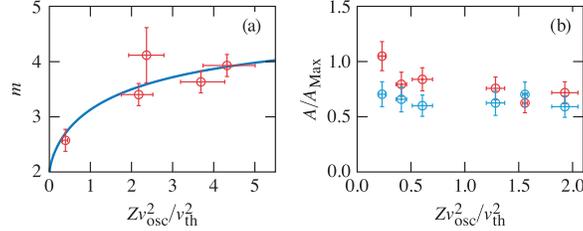
FIG. 3. (a) Measured super-Gaussian order (red points) is compared to Matte's scaling law (blue curve). (b) The measured (red circles) and calculated (blue circles) absorption (Eq. 5), normalized to the absorption calculated assuming a Maxwellian electron distribution function, is plotted as a function of the ratio of the inverse bremsstrahlung heating rate to the electron-electron collision rate determined from the measured plasma conditions at the center of the plasma. Error-bars represent one standard deviation propagated from uncertainties in the measured plasma conditions.

$Z = 25$) were obtained from the simultaneous measurement of the angularly resolved electron plasma wave features [Fig. 1(c)] and collective ion-acoustic wave features (see Supplemental Information B).

Figure 2 shows that the measured electron distribution transitions from a super-Gaussian to a Maxwellian shape at $\sim 3v_{th}$, whereas the theory from Fourkal $et$ $al.$[9] predicts an earlier transition around $\sim 2.5v_{th}$ and more electrons in the tail. This departure of Fourkal from a super-Gaussian distribution was calculated considering a single plane-wave electromagnetic source, where electrons oscillating in the laser field collide with electrons in the tail, modifying the distribution function at high energies. By introducing five overlapped beams, consistent with the experimental configuration, particle simulations using the code $Quartz$ (see Supplemental Information D) show the number of electrons in the tail exceeds the super-Gaussian for velocities in the range $3.5v_{th} \lesssim v \lesssim 4.5v_{th}$, qualitatively consistent with the enhancement above super-Gaussian observed in the data. These results suggest that the increased uniformity due to multiple overlapped beams reduced the energy transferred to the high-velocity electrons.

Figure 3(a) shows the super-Gaussian order, determined by fitting the bulk of the measured distribution, as a function of the ratio of inverse bremsstrahlung heating rate to electron-electron collision rate. The heuristic scaling from Matte $et$ $al.$[7] (Eq. 4) is in good agreement with the measurements. The order of the electron distribution function increases from a Maxwellian ($m = 2$) towards a highly super-Gaussian shape ($m = 5$) as the inverse

8

bremsstrahlung heating of the slow electrons dominates over the thermalization. The ratio of inverse bremsstrahlung heating to electron-electron collision rate was varied by changing the heater beam intensity ($I_{UV}^{total} = 0.62 - 2.8 \times 10^{15}$ W/cm$^2$) and the gas species (hydrogen, nitrogen, argon, and krypton), which resulted in a range of temperatures ($T_e = 0.5 - 1.3$ keV) and ionization states ($Z = 1 - 25$). The electron density was maintained throughout these shots ($n_e \approx 4 \times 10^{19}$ cm$^{-3}$).

Figure 3(b) shows that the measured laser absorption was significantly less than the absorption calculated assuming a plasma with a Maxwellian electron distribution. The absorption rapidly drops to $\sim 60\%$ of the Maxwellian expectation as the relative heating rate increases (large $Zv_{osc}^2/v_{th}^2$). When the inverse bremsstrahlung heating rate dominates over the electron-electron collision rate, the reduction in absorption is in reasonable agreement with the original predictions[1],

$$dA_{SG}(n_e, T_e) = \left[ 1 - \frac{0.553}{1 + (0.27v_{th}^2/Zv_{osc}^2)^{0.75}} \right] \times dA_{Max}(n_e, T_e). \tag{5}$$

where $dA_{Max}$ is the differential absorption calculated assuming a Maxwellian plasma (see Supplemental Information E) and using the plasma conditions determined along the path of the probe beam using spatially resolved Thomson scattering (see Supplemental Information C). The calculated absorption shown in Fig. 3(b) was computed by integrating Eq. 5 over the path of the probe beam.

In inertial confinement fusion plasmas, it has long been assumed that these non-Maxwellian electron distribution functions lead to a reduction in laser heating and in this work this reduction was measured. Furthermore, it was predicted that non-Maxwellian distributions change the plasma wave damping, which results in a redistribution of the thermal energy in the fluctuation spectrum. This affects the atomic transition rates used to describe x-ray spectra[7] and plasma instabilities that grow from thermal noise, which could have a significant impact on predictive capabilities[40–43]. In laser-plasma studies, the agreement between the simple model of a super-Gaussian electron distribution and these measurements in shape (Fig. 2) and scaling (Fig. 3) provides confidence in using this closed form solution in hydrodynamic simulations as a more tractable option compared to Fokker-Planck simulations when the details of the electron distribution function are important. The ability to measure distribution functions opens the scope of investigation to include non-Maxwellian distribution functions, which will improve understanding of plasma physics

9

experiments and provide avenues to grand challenge plasma applications.

--- ---

* Corresponding Author: amild@lle.rochester.edu

[1] A. B. Langdon, Nonlinear inverse bremsstrahlung and heated-electron distributions, Phys. Rev. Lett. **44**, 575–579 (1980).

[2] I. V. Igumenshchev, V. N. Goncharov, W. Seka, D. Edgell, and T. R. Boehly, The effect of resonance absorption in OMEGA direct-drive designs and experiments, Phys. Plasmas **14**, 092701 (2007).

[3] M. D. Rosen, H. A. Scott, D. E. Hinkel, E. A. Williams, D. A. Callahan, R. P. Town, L. Divol, P. A. Michel, W. L. Kruer, L. J. Suter, R. A. London, J. A. Harte, and G. B. Zimmerman,

The role of a detailed configuration accounting (DCA) atomic physics package in explaining the energy balance in ignition-scale hohlraums, High Energy Density Phys. **7**, 180–190 (2011).

[4] W. Davies and S. Ramsden, Scattering of light from the electrons in a plasma, Phys. Lett. **8**, 179–180 (1964).

[5] J. M. Liu, J. S. De Groot, J. P. Matte, T. W. Johnston, and R. P. Drake, Measurements of inverse bremsstrahlung absorption and non-maxwellian electron velocity distributions, Phys. Rev. Lett. **72**, 2717–2720 (1994).

[6] S. H. Glenzer, W. Rozmus, B. J. MacGowan, K. G. Estabrook, J. D. de Groot, G. B. Zimmerman, H. A. Baldis, J. A. Harte, R. W. Lee, E. A. Williams, and B. G. Wilson, Thomson scattering from high-Z laser-produced plasmas, Phys. Rev. Lett. **82**, 97–100 (1999).

[7] J. P. Matte, M. Lamoureux, C. Moller, R. Y. Yin, J. Delettrez, J. Virmont, and T. W. Johnston, Non-Maxwellian electron distributions and continuum X-ray emission in inverse Bremsstrahlung heated plasmas, Plasma Phys. Control. Fusion **30**, 1665–1689 (1988).

[8] S. Brunner and E. Valeo, Simulations of electron transport in laser hot spots, Phys. Plasmas **9**, 923–936 (2002).

[9] E. Fourkal, V. Y. Bychenkov, W. Rozmus, R. Sydora, C. Kirkby, C. E. Capjack, S. H. Glenzer, and H. A. Baldis, Electron distribution function in laser heated plasmas, Phys. Plasmas **8**, 550–556 (2001).

[10] P. Mora and H. Yahi, Thermal heat-flux reduction in laser-produced plasmas, Phys. Rev. A **26**, 2259–2261 (1982).

[11] C. T. Dum, Anomalous heating by ion sound turbulence, Phys. Fluids **21**, 945–955 (1978).

[12] J. Zheng, C. X. Yu, and Z. J. Zheng, Effects of non-Maxwellian (super-Gaussian) electron velocity distribution on the spectrum of Thomson scattering, Phys. Plasmas **4**, 2736–2740 (1997).

[13] M. Krook and T. T. Wu, Formation of maxwellian tails, Phys. Rev. Lett. **36**, 1107–1109 (1976).

[14] D. H. Froula, S. H. Glenzer, N. C. Luhmann, Jr., and J. Sheffield, *Plasma Scattering of Electromagnetic Radiation: Theory and Measurement Techniques*, 2nd ed. (Academic Press, Amsterdam, 2011).

[15] D. R. Farley, K. G. Estabrook, S. G. Glendinning, S. H. Glenzer, B. A. Remington, K. Shigemori, J. M. Stone, R. J. Wallace, G. B. Zimmerman, and J. A. Harte, Radiative jet experiments

of astrophysical interest using intense lasers, Phys. Rev. Lett. **83**, 1982–1985 (1999).

[16] D. Montgomery, R. Johnson, J. Cobble, J. Fernández, E. Lindman, H. Rose, and K. Estabrook, Characterization of plasma and laser conditions for single hot spot experiments, Laser Part. Beams **17**, 349–359 (1999).

[17] T. E. Tierney IV, D. S. Montgomery, J. F. Benage, F. J. Wysocki, and M. S. Murillo, Modelling of collective Thomson scattering from collisional plasmas, J. Phys. A: Math. Gen. **36**, 5981–5989 (2003).

[18] S. V. Lebedev, L. Suttle, G. F. Swadling, M. Bennett, S. N. Bland, G. C. Burdiak, D. Burgess, J. P. Chittenden, A. Ciardi, A. Clemens, P. De Grouchy, G. N. Hall, J. D. Hare, N. Kalmoni, N. Niasse, S. Patankar, L. Sheng, R. A. Smith, F. Suzuki-Vidal, J. Yuan, A. Frank, E. G. Blackman, and R. P. Drake, The formation of reverse shocks in magnetized high energy density supersonic plasma flows, Phys. Plasmas **21**, 056305 (2014).

[19] G. F. Swadling, S. V. Lebedev, A. J. Harvey-Thompson, W. Rozmus, G. Burdiak, L. Suttle, S. Patankar, R. A. Smith, M. Bennett, G. N. Hall, F. Suzuki-Vidal, S. Bland, and J. Yuan, Interpenetration and deflection phenomena in collisions between supersonic, magnetized, tungsten plasma flows diagnosed using high resolution optical Thomson scattering, Phys. Plasmas **22**, 072706 (2015).

[20] J. S. Ross, S. H. Glenzer, J. P. Palastro, B. B. Pollock, D. Price, G. R. Tynan, and D. H. Froula, Thomson-scattering measurements in the collective and noncollective regimes in laser produced plasmas, Rev. Sci. Instruments **81**, 10D523 (2010).

[21] N. J. Peacock, D. C. Robinson, M. J. Forrest, P. D. Wilcock, and V. V. Sannikov, Measurement of the electron temperature by Thomson scattering in Tokamak T3, Nature **224**, 488–490 (1969).

[22] J. C. Valenzuela, C. Krauland, D. Mariscal, I. Krasheninnikov, C. Niemann, T. Ma, P. Mabey, G. Gregori, P. Wiewior, A. M. Covington, and F. N. Beg, Measurement of temperature and density using non-collective X-ray Thomson scattering in pulsed power produced warm dense plasmas, Sci. Reports **8**, 8432 (2018).

[23] S. Frydrych, J. Vorberger, N. J. Hartley, A. K. Schuster, K. Ramakrishna, A. M. Saunders, T. van Driel, R. W. Falcone, L. B. Fletcher, E. Galtier, E. J. Gamboa, S. H. Glenzer, E. Granados, M. J. MacDonald, A. J. MacKinnon, E. E. McBride, I. Nam, P. Neumayer, A. Pak, K. Voigt, M. Roth, P. Sun, D. O. Gericke, T. Döppner, and D. Kraus, Demonstra-

tion of X-ray Thomson scattering as diagnostics for miscibility in warm dense matter, Nat. Commun. **11**, 2620 (2020).

[24] G. Gregori, S. H. Glenzer, F. J. Rogers, S. M. Pollaine, O. L. Landen, C. Blancard, G. Faussurier, P. Renaudin, S. Kuhlbrodt, and R. Redmer, Electronic structure measurements of dense plasmas, Phys. Plasmas **11**, 2754–2762 (2004).

[25] A. C. A. P. Van Lammeren, C. J. Barth, Q. C. Van Est, and F. C. Schüller, Non-Maxwellian electron velocity distributions observed with Thomson scattering in the TORTUR tokamak, Nucl. Fusion **32**, 655 (1992).

[26] T. Hori, M. D. Bowden, K. Uchino, and K. Muraoka, Measurement of non-Maxwellian electron energy distributions in an inductively coupled plasma, Appl. Phys. Lett. **69**, 3683 (1996).

[27] S. E. Serge, and L. Pieroni, Measurement of non-Maxwellian electron distribution functions in hot plasma and the importance for Thomson scattering diagnostics, Phys. Lett. A **51**, 25 (1974).

[28] A. L. Milder, S. T. Ivancic, J. P. Palastro, and D. H. Froula, Impact of non-Maxwellian electron velocity distribution functions on inferred plasma parameters in collective Thomson scattering, Phys. Plasmas **26**, 022711 (2019).

[29] D. Turnbull, A. Colaïtis, A. M. Hansen, A. L. Milder, J. P. Palastro, J. Katz, C. Dorrer, B. E. Kruschwitz, D. J. Strozzi, and D. H. Froula, Impact of the Langdon effect on crossed-beam energy transfer, Nat. Phys. **16**, 181–185 (2020).

[30] R. J. Henchen, M. Sherlock, W. Rozmus, J. Katz, D. Cao, J. P. Palastro, and D. H. Froula, Observation of Nonlocal Heat Flux Using Thomson Scattering, Phys. Rev. Lett. **121**, 125001 (2018).

[31] C. Zhang, C. K. Huang, K. A. Marsh, C. E. Clayton, W. B. Mori, and C. Joshi, Ultrafast optical field-ionized gases-A laboratory platform for studying kinetic plasma instabilities, Sci. Adv. **5**, eaax4545 (2019).

[32] M. Salewski, S. K. Nielsen, H. Bindslev, V. Furtula, N. N. Gorelenkov, S. B. Korsholm, F. Leipold, F. Meo, P. K. Michelsen, D. Moseev, and M. Stejner, On velocity space interrogation regions of fast-ion collective Thomson scattering at ITER, Nucl. Fusion **51**, 083014 (2011).

[33] H. Bindslev, J. A. Hoekzema, J. Egedal, J. A. Fessey, T. P. Hughes, and J. S. Machuzak, Fast-ion velocity distributions in jet measured by collective thomson scattering, Phys. Rev.

Lett. **83**, 3206–3209 (1999).

[34] K. V. Beausang, S. L. Prunty, R. Scannell, M. N. Beurskens, M. J. Walsh, E. de La Luna, and JET EFDA Contributors, Detecting non-Maxwellian electron velocity distributions at JET by high resolution Thomson scattering, Rev. Sci. Instrum **82**, 033514 (2011).

[35] T. R. Boehly, R. S. Craxton, T. H. Hinterman, J. H. Kelly, T. J. Kessler, S. A. Kumpan, S. A. Letzring, R. L. McCrory, S. F. B. Morse, W. Seka, S. Skupsky, J. M. Soures, and C. P. Verdon, The upgrade to the OMEGA laser system, Rev. Sci. Instruments **66**, 508–510 (1995).

[36] A. M. Hansen, D. Haberberger, J. Katz, D. Mastrosimone, R. K. Follett, and D. H. Froula, Supersonic gas-jet characterization with interferometry and Thomson scattering on the OMEGA Laser System, Rev. Sci. Instruments **89**, 10C103 (2018).

[37] J. Katz, D. Turnbull, B. Kruschwitz, A. Rigatti, R. Rinefierd, and D. H. Froula, A transmitted beam diagnostic for the wavelength tunable UV drive beam on OMEGA, Rev. Sci. Instruments , *(In Review)* (2021).

[38] J. P. Palastro, J. S. Ross, B. Pollock, L. Divol, D. H. Froula, and S. H. Glenzer, Fully relativistic form factor for Thomson scattering, Phys. Rev. E **81**, 036411 (2010).

[39] *fmincon Function, MATLAB **R**2015b, The MathWorks Inc., Natick, MA 01760-2098*.

[40] W. Rozmus, T. Chapman, A. Brantov, B. J. Winjum, R. L. Berger, S. Brunner, V. Y. Bychenkov, A. Tableman, M. Tzoufras, and S. Glenzer, Resonance between heat-carrying electrons and Langmuir waves in inertial confinement fusion plasmas, Phys. Plasmas **23**, 012707 (2016).

[41] D. J. Strozzi, D. S. Bailey, P. Michel, L. Divol, S. M. Sepke, G. D. Kerbel, C. A. Thomas, J. E. Ralph, J. D. Moody, and M. B. Schneider, Interplay of Laser-Plasma Interactions and Inertial Fusion Hydrodynamics, Phys. Rev. Lett. **118**, 025002 (2017).

[42] B. B. Afeyan, A. E. Chou, and W. L. Kruer, Effects of Non-Maxwellian Electron Velocity Distributions on Parametric Instabilities, *ICF Quarterly Report*, 78–85 , Lawrence Livermore National Laboratory, Livermore, CA, Report UCRL-LR-105821-97-2, (1998).

[43] J. L. Kline, D. S. Montgomery, B. Bezzerides, J. A. Cobble, D. F. Dubois, R. P. Johnson, H. A. Rose, L. Yin, and H. X. Vu, Observation of a transition from fluid to kinetic nonlinearities for langmuir waves driven by stimulated raman backscatter, Phys. Rev. Lett. **94**, 175003 (2005).

[44] R. K. Follett, J. A. Delettrez, D. H. Edgell, R. J. Henchen, J. Katz, J. F. Myatt, and D. H. Froula, Plasma characterization using ultraviolet Thomson scattering from ion-acoustic and

electron plasma waves, Rev. Sci. Instruments **87**, 11E401 (2016).

[45] J. Katz, R. Boni, C. Sorce, R. Follett, M. J. Shoup, and D. H. Froula, A reflective optical transport system for ultraviolet Thomson scattering from electron plasma waves on OMEGA, Rev. Sci. Instruments **83**, 10E349 (2012).

[46] M. Sherlock, J. P. Brodrick, and C. P. Ridgers, A comparison of non-local electron transport models for laser-plasmas relevant to inertial confinement fusion, Phys. Plasmas **24**, 082706 (2017).

[47] A. R. Bell, A. P. Robinson, M. Sherlock, R. J. Kingham, and W. Rozmus, Fast electron transport in laser-produced plasmas and the KALOS code for solution of the Vlasov-Fokker-Planck equation, Plasma Phys. Control. Fusion **48**, R37–R57 (2006).

[48] J. Garnier and L. Videau, Statistical analysis of the sizes and velocities of laser hot spots of smoothed beams, Phys. Plasmas **8**, 4914–4924 (2001).

[49] T. Takizuka and H. Abe, A binary collision model for plasma simulation with a particle code, J. Comput. Phys. **25**, 205–219 (1977).

[50] W. L. Kruer, *The Physics Of Laser Plasma Interaction*, 1st ed. (CRC Press, 2003).